Observation of the decay $\psi(3686) \to \Sigma^0\bar{\Sigma}^0\omega$

M. Ablikim *et al.*[*]
(BESIII Collaboration)

(Received 25 March 2025; accepted 1 May 2025; published 12 May 2025; corrected 6 June 2025)

Using a dataset of $(27.12 \pm 0.14) \times 10^8$ $\psi(3686)$ events collected by the BESIII detector operating at the BEPCII collider, we report the first observation of the decay $\psi(3686) \to \Sigma^0\bar{\Sigma}^0\omega$ with a statistical significance of 8.9σ. The measured branching fraction is $(1.24 \pm 0.16_{\rm stat} \pm 0.11_{\rm sys}) \times 10^{-5}$, where the first uncertainty is statistical and the second is systematic. Additionally, we investigate potential intermediate states in the invariant mass distributions of $\Sigma^0\omega$, $\bar{\Sigma}^0\omega$ and $\Sigma^0\bar{\Sigma}^0$. A hint of a resonance is observed in the invariant mass distribution of $M_{\Sigma^0(\bar{\Sigma}^0)\omega}$, located around 2.06 GeV$/c^2$, with a significance of 2.5σ.

DOI: 10.1103/PhysRevD.111.092007

I. INTRODUCTION

The existing theoretical framework of Quantum Chromodynamics (QCD) successfully describes strong interactions between quarks and gluons in the perturbative regime. However, precise calculations in the nonperturbative regime remain challenging and often depend on effective theories and approximations. Charmonium decays, which straddle the perturbative and nonperturbative regimes, provide an ideal laboratory for testing QCD theories [1,2].

In addition to advancing our understanding of charmonium states, studying charmonium decays also facilitates the search for excited baryon resonances. Investigating the hadronic three-body final states of $\psi(3686)$ decays, such as $\psi(3686) \to B\bar{B}P(V)$, where B denotes a baryon, $\bar{B}$ its antiparticle, and $P(V)$ a pseudoscalar (vector) meson, is crucial for discovering excited baryons predicted by effective field theories but yet to be observed [3,4]. Notably, experimental data on excited hyperon resonances, such as Λ^* and Σ^*, are significantly sparser compared to those for baryons with zero strangeness [5]. Therefore, experimental confirmation or exclusion of these predicted hyperons is essential for advancing hyperon spectroscopy.

In recent years, the BESIII collaboration has reported observations or evidence of several excited Λ^* states via $\psi(3686) \to B\bar{B}P(V)$ decays. For example, the $\Lambda(1670)$ is observed with a significance larger than 5.0σ in the decay $\psi(3686) \to \Lambda\bar{\Lambda}\eta$ [6]. Evidence of an excited state Λ^* is found in $\psi(3686) \to \Lambda\bar{\Lambda}\omega$ with a significance of 3.0σ [7]. Additionally, a near-threshold enhancement in $\Lambda\bar{\Lambda}$ is observed for the first time in $e^+e^- \to \Lambda\bar{\Lambda}\phi$ [8]. These findings motivate the search for excited Σ^* states in the analogous three-body decay $\psi(3686) \to \Sigma^0\bar{\Sigma}^0\omega$.

In this paper, we report the first observation and branching fraction measurement of the decay $\psi(3686) \to \Sigma^0\bar{\Sigma}^0\omega$, using $(27.12 \pm 0.14) \times 10^8$ $\psi(3686)$ events [9]. We also search for potential structures in the invariant mass distributions of $\Sigma^0\omega$, $\bar{\Sigma}^0\omega$ and $\Sigma^0\bar{\Sigma}^0$.

II. BESIII DETECTOR AND MONTE CARLO SIMULATION

The BESIII detector [10] records symmetric e^+e^- collisions provided by the BEPCII storage ring [11] in the center-of-mass energy range from 1.84 to 4.95 GeV. The peak luminosity of 1.1×10^{33} cm^{-2} s^{-1} is achieved at $\sqrt{s} = 3.773$ GeV. BESIII has collected large data samples in this energy region [12,13]. The cylindrical core of the BESIII detector covers 93% of the full solid angle and consists of a helium-based multilayer drift chamber (MDC), a time-of-flight system (TOF), and a CsI (Tl) electromagnetic calorimeter (EMC), which are all enclosed in a superconducting solenoidal magnet providing a 1.0 T magnetic field. Modules of the resistive plate muon counter (MUC) are embedded in an octagonal flux-return yoke supporting the superconducting solenoid. The charged-particle momentum resolution at 1 GeV$/c$ is 0.5%, and the specific ionization energy loss d$E/$dx resolution is 6% for the electrons from Bhabha scattering at 1 GeV. The EMC measures photon energy with a resolution of 2.5% (5%) at 1 GeV in the barrel (end cap) region. The time resolution of the TOF plastic scintillator barrel part is 68 ps, while that of the end cap part is 110 ps. The end cap TOF system was upgraded in 2015 using multigap resistive plate chamber technology, providing a time resolution

[*]Full author list given at the end of the article.

Published by the American Physical Society under the terms of the Creative Commons Attribution 4.0 International license. Further distribution of this work must maintain attribution to the author(s) and the published article's title, journal citation, and DOI. Funded by SCOAP[3].

of 60 ps, which benefits ~83% of the data used in this analysis [14–16].

Monte Carlo (MC) simulated data samples produced with Geant4-based software [17], which includes the geometric description [18] of the BESIII detector and the detector response, are used to optimize the event selection criteria, determine the detection efficiencies and study the background components. The simulation models the beam energy spread and initial-state radiation in the e^+e^- annihilations using the generator KKMC [19,20]. The inclusive MC sample includes the production of the $\psi(3686)$ resonance, the initial-state radiation production of J/ψ, and the continuum processes incorporated in KKMC. All particle decays are modeled by EvtGen [21,22] using branching fractions either taken from the Particle Data Group (PDG) [23], when available, or otherwise estimated with Lundcharm [24,25]. Final state radiation from charged final state particles is included using PHOTOS [26]. The signal MC sample of $\psi(3686) \to \Sigma^0\bar{\Sigma}^0\omega$, comprising 3.0×10^6 events, is generated with an uniform phase space (PHSP) distribution. The decays $\Sigma^0 \to \gamma\Lambda(\Lambda \to p\pi^-)$ and $\bar{\Sigma}^0 \to \gamma\bar{\Lambda}(\bar{\Lambda} \to \bar{p}\pi^+)$ are also simulated using the PHSP model [27], and the decay of ω is modeled using OMEGA_DALITZ generator [22]. The data sample collected at the center-of-mass energy of $\sqrt{s} = 3.650$ GeV, with an integrated luminosity of 401 pb^{-1} [9], is used to investigate the continuum background.

III. EVENT SELECTION AND BACKGROUND ANALYSIS

To reconstruct the signal decay, we select the decay chains $\Sigma^0 \to \gamma\Lambda$, $\Lambda \to p\pi^-$, $\bar{\Sigma}^0 \to \gamma\bar{\Lambda}$, $\bar{\Lambda} \to \bar{p}\pi^+$ and $\omega \to \pi^+\pi^-\pi^0$ with $\pi^0 \to \gamma\gamma$. Each candidate event must contain at least three positive and three negative charged tracks and a minimum of four photons. Additionally, charged tracks detected in the MDC must satisfy $|\cos\theta| \leq 0.93$, where θ is the polar angle relative to the z-axis, the symmetry axis of the MDC.

Photon candidates are identified from showers in the EMC. The deposited energy of each shower is required to exceed 25 MeV in the barrel region ($|\cos\theta| < 0.80$) or 50 MeV in the end cap region ($0.86 < |\cos\theta| < 0.92$). To reduce electronic noise and energy depositions unrelated to the event, the EMC cluster time, measured from the reconstructed event start time, must lie within [0, 700] ns. To exclude showers that originate from charged tracks, the angle subtended by the EMC shower and the position of the closest charged track at the EMC must be greater than 10 degrees as measured from the interaction point (IP).

Particle identification (PID) for charged tracks combines measurements of $\mathrm{d}E/\mathrm{d}x$ in the MDC and the flight time in the TOF to calculate the probability $P(h)$ for each particle type hypothesis, where ($h = p, K, \pi$). Tracks are assigned as (anti-)proton candidates if they satisfy $P(p) > P(K)$ and $P(p) > P(\pi)$. Each candidate event must include at least one proton and one antiproton. To account for antiproton interactions with detector materials, the opening angle between the antiproton trajectory and any photon shower must exceed 20 degrees.

The $\Lambda(\bar{\Lambda})$ candidates are reconstructed by combining identified (anti)protons with oppositely charged tracks and performing a secondary vertex fit. If multiple combinations satisfy the fit, the one that minimizes $(M_{p\pi^-} - m_\Lambda)^2 + (M_{\bar{p}\pi^+} - m_{\bar{\Lambda}})^2$ is selected, where $M_{p\pi^-}(M_{\bar{p}\pi^+})$ is the invariant mass of the $p\pi^-(\bar{p}\pi^+)$ pair, and $m_\Lambda(m_{\bar{\Lambda}})$ is the nominal mass [23] of $\Lambda(\bar{\Lambda})$. The decay length of $\Lambda(\bar{\Lambda})$, defined as the distance from the $\Lambda(\bar{\Lambda})$ decay vertex to the IP, must be greater than zero. Reconstructed Λ and $\bar{\Lambda}$ candidates must satisfy $|M_{p\pi^-(\bar{p}\pi^+)} - m_{\Lambda(\bar{\Lambda})}| < 0.01$ GeV$/c^2$ (five standard deviations), as illustrated in Fig. 1.

For the remaining charged tracks not involved in reconstructing Λ and $\bar{\Lambda}$, we assume they are pions originating from the ω decay. These tracks must satisfy $|V_z| < 10$ cm and $|V_{xy}| < 1$ cm, where $|V_z|$ is the distance of closest approach to the IP along the z direction and V_{xy} is the distance in the transverse xy plane. A vertex fit is

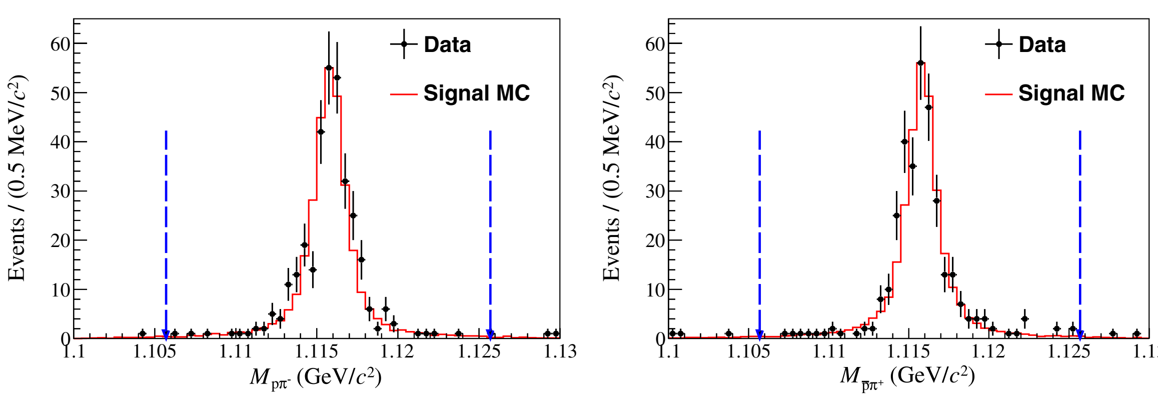

FIG. 1. Distributions of (left) $M_{p\pi^-}$ and (right) $M_{\bar{p}\pi^+}$. The dots with error bars are data, the red solid lines represent the normalized signal MC sample, and the blue dashed lines indicate the required mass ranges.

performed on each $\pi^+\pi^-$ pairs to ensure a common decay vertex.

In order to improve the invariant mass resolution and reduce the backgrounds, a five-constraint (5C) kinematic fit is applied to each $\psi(3686) \to \Lambda\bar{\Lambda}\pi^+\pi^-4\gamma$ candidate, enforcing energy-momentum conservation and constraining photon pairs to the nominal π^0 mass. The combination with the smallest χ^2_{5C} is selected, requiring $\chi^2_{5C} < 60$. This criterion is optimized using a figure-of-merit defined as $\frac{S}{\sqrt{S+B}}$, where S is the normalized number of signal events in the signal MC sample and B is the number of background events in the inclusive MC sample. To suppress backgrounds with different photon multiplicities than the signal decay, a four-constraint (4C) kinematic fit is applied to $\Lambda\bar{\Lambda}\pi^+\pi^-4\gamma$, $\Lambda\bar{\Lambda}\pi^+\pi^-3\gamma$ and $\Lambda\bar{\Lambda}\pi^+\pi^-5\gamma$ combinations (if more than four photons are present in the event), requiring $\chi^2_{4C}(\Lambda\bar{\Lambda}\pi^+\pi^-4\gamma) < \chi^2_{4C}(\Lambda\bar{\Lambda}\pi^+\pi^-3\gamma)$ and $\chi^2_{4C}(\Lambda\bar{\Lambda}\pi^+\pi^-4\gamma) < \chi^2_{4C}(\Lambda\bar{\Lambda}\pi^+\pi^-5\gamma)$.

In the signal decay, the Σ^0 and $\bar{\Sigma}^0$ states always appear in pairs and the relevant photons are expected to yield $M_{\gamma^i\Lambda}$ close to $M_{\gamma^j\bar{\Lambda}}$, where $M_{\gamma^i\Lambda}$ and $M_{\gamma^j\bar{\Lambda}}$ are the invariant masses of $\gamma^i\Lambda$ and $\gamma^j\bar{\Lambda}$, respectively. Here, γ^i and γ^j are different photons not involved in reconstructing π^0. We select the photon candidate by minimizing the variable $\Delta = (M_{\gamma^i\Lambda} - M_{\gamma^j\bar{\Lambda}})^2$.

To veto backgrounds from the decay $\psi(3686) \to \pi^+\pi^-(\pi^0\pi^0)J/\psi$, we require the recoil mass of $\pi^+\pi^-(\pi^0\gamma^i\gamma^j)$ to be outside of the J/ψ mass window. The mass window is set at $[3.089, 3.105]$ GeV$/c^2$ for $\psi(3686) \to \pi^+\pi^-J/\psi$ and adjusted to $[3.090, 3.145]$ GeV$/c^2$ for $\psi(3686) \to \pi^0\pi^0 J/\psi$.

Background candidates are studied using the $\psi(3686)$ inclusive MC sample with the TopoAna package [28]. Within the fit range of $[0.65, 0.95]$ GeV$/c^2$, no peaking background is observed in the $M_{\pi^+\pi^-\pi^0}$ spectrum. The remaining dominant background events are $\psi(3686) \to \pi^+\pi^-J/\psi, J/\psi \to \pi^0\Sigma^0\bar{\Sigma}^0$. Continuum background candidates, estimated using off-resonance data at $\sqrt{s} = 3.650$ GeV, are negligible.

IV. BRANCHING FRACTION MEASUREMENT

After applying all selection criteria, we fit the spectra of $M_{\gamma^i\Lambda}$, $M_{\gamma^j\bar{\Lambda}}$, and $M_{\pi^+\pi^-\pi^0}$ to determine the signal and sideband regions, as detailed in Table I. The signal events

TABLE I. Signal and sideband regions of Σ^0, $\bar{\Sigma}^0$, and ω.

	Signal region (GeV$/c^2$)	Sideband region (GeV$/c^2$)
$M_{\gamma^i\Lambda}$	[1.176, 1.204]	[1.223, 1.251]
$M_{\gamma^j\bar{\Lambda}}$	[1.175, 1.204]	[1.224, 1.253]
$M_{\pi^+\pi^-\pi^0}$	[0.758, 0.822]	[0.630, 0.694], [0.886, 0.950]

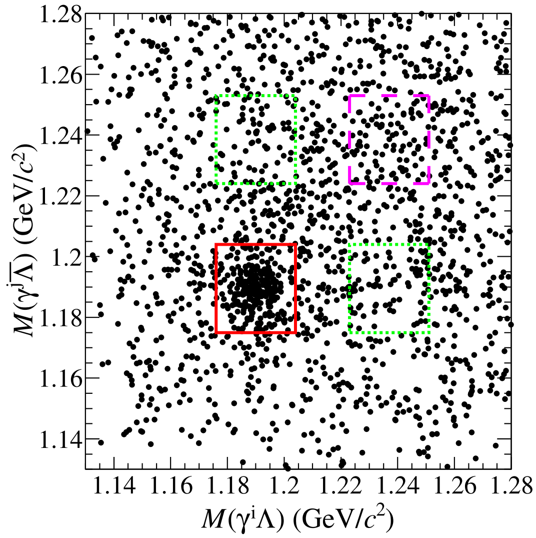

FIG. 2. Distribution of $M_{\gamma^i\Lambda}$ versus $M_{\gamma^j\bar{\Lambda}}$ in the data. Events are within the ω mass window. The red solid box indicates the signal region, the green dashed boxes denote the 1-D sideband regions, and the magenta long dashed box represents the $\Sigma^0 - \bar{\Sigma}^0$ sideband region.

of Σ^0 and $\bar{\Sigma}^0$ are distinctly visible in the scatter plot of $M_{\gamma^i\Lambda}$ versus $M_{\gamma^j\bar{\Lambda}}$, as illustrated in Fig. 2.

The signal yield of the decay $\psi(3686) \to \Sigma^0\bar{\Sigma}^0\omega$ is extracted using an extended unbinned maximum likelihood fit [29] to the $M_{\pi^+\pi^-\pi^0}$ spectrum, considering only events within the 2-D $\Sigma^0\bar{\Sigma}^0$ signal region. The ω signal is described with the signal MC simulated shape [30] and the smooth background contribution is modeled with a second-order Chebyshev polynomial function.

The fit result is shown in Fig. 3. The events from the 2-D sideband are overlayed to confirm the absence of any

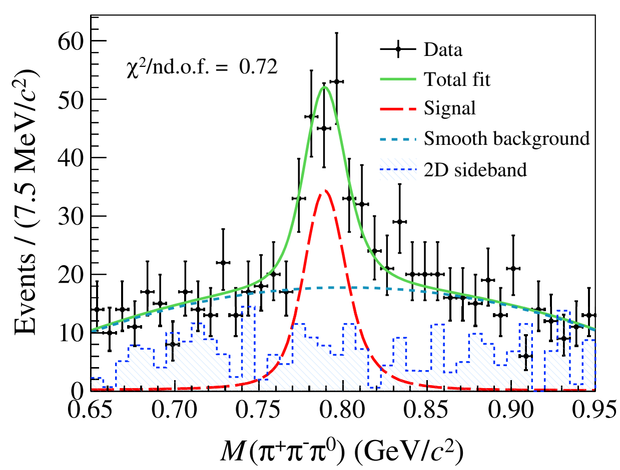

FIG. 3. Fit to the $M_{\pi^+\pi^-\pi^0}$ distribution. The dots with error bars are data, the grass green solid line denotes the fit result, the red long dashed line represents the signal component, the blue dashed line is smooth background, and the light blue shadowed area represents the smooth 2-D sideband of Σ^0 and $\bar{\Sigma}^0$.

TABLE II. Signal yield, statistical significance, efficiency and measured branching fraction. The uncertainties are statistical only.

Signal yield	Significance	$\varepsilon(\%)$	$\mathcal{B}(\times 10^{-5})$
171.7 ± 22.3	8.9σ	0.57	1.24 ± 0.16

peaking background contribution. From this fit, the number of signal events is determined to be 171.7 ± 22.3. The uncertainty is statistical only. The statistical significance, estimated from the difference in the log-likelihood values with and without the signal component, is 8.9σ. The branching fraction is calculated as

$$\mathcal{B}(\psi(3686) \to \Sigma^0\bar{\Sigma}^0\omega) = \frac{N_{\rm sig}^{\rm obs}}{N_{\psi(3686)} \cdot \varepsilon_{\rm sig} \cdot \mathcal{B}_\omega}, \quad (1)$$

where $N_{\rm sig}^{\rm obs}$ is the signal yield, $\mathcal{B}_\omega$ is the branching fraction of $\omega \to \pi^+\pi^-\pi^0$ [23], $\varepsilon_{\rm sig}$ represents the signal efficiency determined by MC simulation, and $N_{\psi(3686)} = (27.12 \pm 0.14) \times 10^8$ [9] is the total number of $\psi(3686)$ events in the data. The branching fraction of $\Sigma^0 \to \gamma\Lambda$ is 100% according to the PDG, and therefore not included in Eq. (1). The branching fractions of $\Lambda \to p\pi^-$, $\bar{\Lambda} \to \bar{p}\pi^+$ and $\pi^0 \to \gamma\gamma$ are incorporated into the signal efficiency. Table II includes the numerical results of the branching fraction measurement.

V. STUDY OF INTERMEDIATE STATES

The distributions of $M_{\Sigma^0\omega}$, $M_{\bar{\Sigma}^0\omega}$ and $M_{\Sigma^0\bar{\Sigma}^0}$, along with the Dalitz plot of $M^2_{\Sigma^0\omega}$ versus $M^2_{\bar{\Sigma}^0\omega}$ presented in Fig. 4 are used to explore the potential intermediate states. Differences between the data and the MC simulation are observed in the $M_{\Sigma^0\omega}$ and $M_{\bar{\Sigma}^0\omega}$ distributions, as well as in the uneven distribution of the Dalitz plot.

To extract potential structure in the $M_{\Sigma^0\omega}$ and $M_{\bar{\Sigma}^0\omega}$ distributions, it is crucial to account for reflections from the charge-conjugate channels. Particularly, we compare $M_{\Sigma^0\omega}$ and $M_{\bar{\Sigma}^0\omega}$ in each event and retain only one of them, denoted as $M_{\Sigma^0(\bar{\Sigma}^0)\omega}$. First, we examine the distribution for the larger value of $M_{\Sigma^0\omega}$ or $M_{\bar{\Sigma}^0\omega}$ (Fig. 5) finding no evidence of a structure. Later, the distribution of $M_{\Sigma^0\omega}$ or $M_{\bar{\Sigma}^0\omega}$ corresponding to the smaller value (Fig. 6) is retained for further analysis.

In Fig. 6, a structure near 2.06 GeV$/c^2$ is evident. To analyze this feature, an unbinned extended maximum likelihood fit is applied to the $M_{\Sigma^0(\bar{\Sigma}^0)\omega}$ spectrum. In the

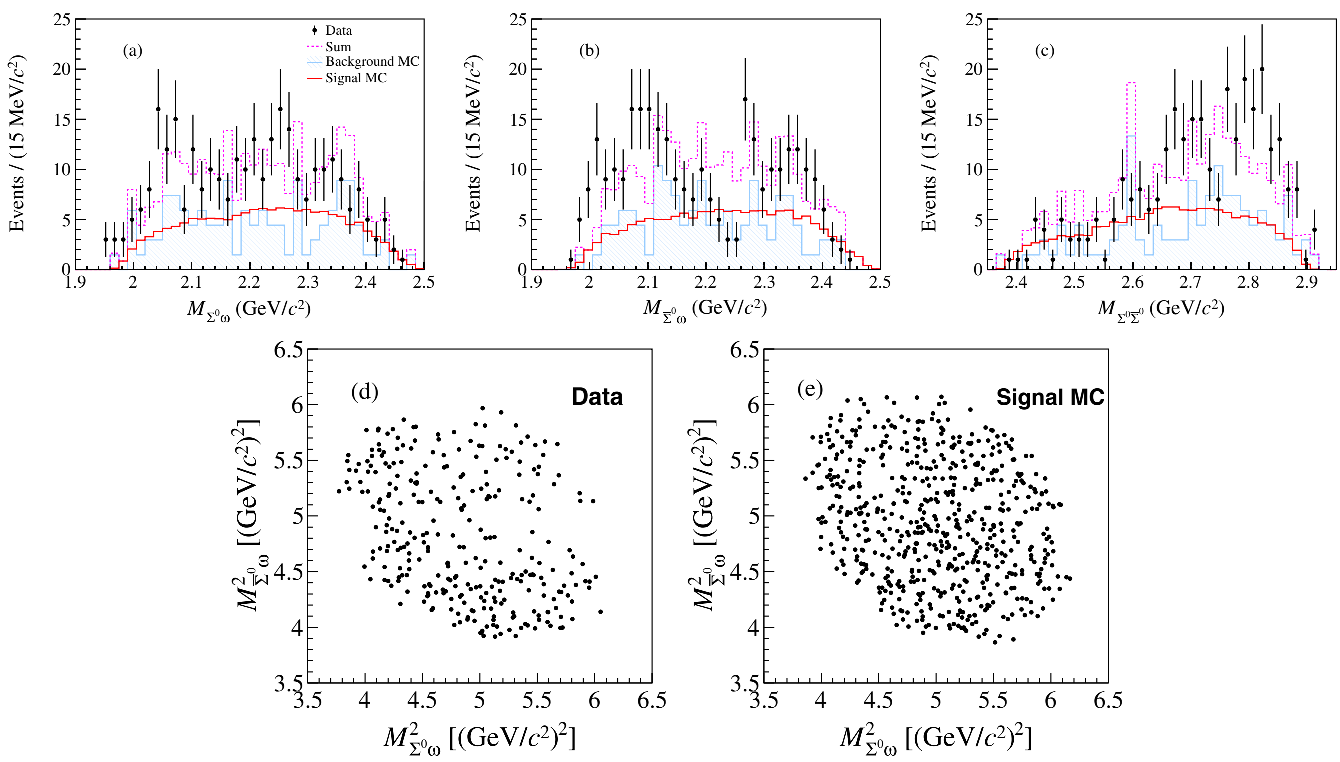

FIG. 4. Top: distributions of (a) $M_{\Sigma^0\omega}$, (b) $M_{\bar{\Sigma}^0\omega}$, and (c) $M_{\Sigma^0\bar{\Sigma}^0}$ in the data and MC samples. The black dots with error bars represent the data, the red solid lines indicate the PHSP signal MC simulated shapes, the shaded blue areas depict the simulated background events derived from the inclusive MC sample and the magenta dashed lines represent the sum of signal and background MC shapes. The numbers of signal and background events are normalized to their respective values in the data. Bottom: Dalitz plot of $M^2_{\Sigma^0\omega}$ versus $M^2_{\bar{\Sigma}^0\omega}$ in the (d) data and (e) signal MC sample. The number of events in the signal MC sample is normalized to twice of the data.

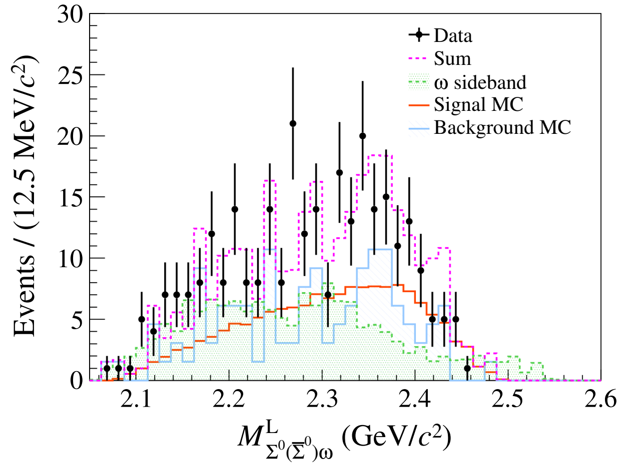

FIG. 5. Distributions of $M^L_{\Sigma^0(\bar{\Sigma}^0)\omega}$ in the data and MC samples; the superscript "L" denotes selecting the larger value between $M_{\Sigma^0\omega}$ and $M_{\bar{\Sigma}^0\omega}$, which is excluded from further analysis. The dots with error bars are the data, the green shaded histogram indicates the ω sideband, the light blue shaded histogram represents the simulated backgrounds derived from the inclusive MC sample, the red solid line depicts the PHSP signal MC shape and the magenta dashed line represents the sum of signal and background MC shapes. The numbers of events are normalized to the data determined by the fit to the $M_{\pi^+\pi^-\pi^0}$ spectrum.

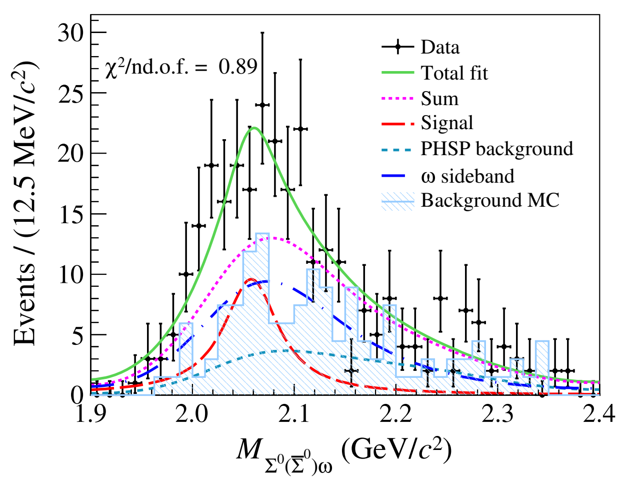

FIG. 6. Fit to the $M_{\Sigma^0(\bar{\Sigma}^0)\omega}$ spectrum, retaining the smaller mass value. The grass green solid line is the fit result, the red long dashed line represents the signal function, the dark blue long dash-dotted line depicts the ω sideband, the light blue dashed line indicates the PHSP MC shape, the magenta short dashed line represents the sum of the sideband and PHSP MC shape, and the light blue shaded histogram represents the simulated backgrounds.

fit, the PHSP shape is derived from the exclusive MC simulation of $\psi(3686) \to \Sigma^0\bar{\Sigma}^0\omega$. The signal function is modeled by a relativistic Breit-Wigner function, defined as

$$|BW(M)|^2 = \frac{k}{(M^2 - m_0^2)^2 + m_0^2\Gamma^2}, \tag{2}$$

where k is a normalization factor, M corresponds to $M_{\Sigma^0(\bar{\Sigma}^0)\omega}$, and m_0 and Γ are the mass and width of the resonance, respectively. For simplicity, the relatively smooth efficiency curve of the signal process is not incorporated into the signal function. The number of non-ω events is fixed according to the previous fit result. Two options are considered to describe the background contribution: a sum of background candidates in the inclusive MC sample, which yields a significance of 5.1σ; or the ω sideband from the data, which yields a significance of 3.1σ. To be conservative, we adopt the latter as the nominal one. The simulated background events are not included in the fit. It is presented in Fig. 6 for comparison. In order to estimate the significance of the intermediate state, we consider uncertainties arising from the background shape, the signal function, and the number of non-ω events. To take into account the uncertainties, the alternative fits are performed. The background events obtained from the ω sideband are changed by increasing the sideband range to 1.5 times its original width. The signal function is smeared with a free Gaussian function. The number of non-ω events, fixed in the fit, is varied by one standard deviation. As a conservative estimation, the smallest significance among these fits is retained. By taking into account the systematic uncertainties and the look-elsewhere effect [31], the global significance of this resonance is 2.5σ.

According to the fit, the mass and width of this structure are (2058 ± 15) MeV$/c^2$ and (65 ± 18) MeV, respectively. Since its significance is less than 3σ, we refrain from reporting an upper limit for the branching fraction of $\mathcal{B}(\psi(3686) \to \Sigma^0 X + \text{c.c.} \to \Sigma^0\bar{\Sigma}^0\omega)$, where X denotes the potential intermediate state.

The observed deviation in the $M_{\Sigma^0(\bar{\Sigma}^0)\omega}$ spectrum suggests the possible presence of an intermediate state. However, the current data statistics is insufficient to confirm its existence or to determine its quantum numbers. Detailed studies with larger datasets and improved model are necessary to verify this resonance.

VI. SYSTEMATIC UNCERTAINTIES

The sources of systematic uncertainty in the branching fraction measurement are described as below and summarized in Table III. Assuming all uncertainties arise from independent sources, the total systematic uncertainty is determined to be 9.2%, by summing the individual contributions in quadrature.

The uncertainty associated with pion tracking is assigned as 1.0% per pion, according to the studies of the control samples $J/\psi \to K^*\bar{K}$ and $J/\psi \to p\bar{p}\pi^+\pi^-$ [32]. The uncertainty is only assigned to the charged pions originating from the ω.

The uncertainty from photon reconstruction is assigned as 0.5% per photon, based on the study of the control sample $e^+e^- \to \gamma\mu^+\mu^-$ [33].

TABLE III. Relative systematic uncertainties for the branching fraction measurement of $\psi(3686) \to \Sigma^0\bar{\Sigma}^0\omega$.

Source	Uncertainty in (%)
Tracking	2.0
Photon reconstruction	2.0
π^0 reconstruction	1.0
$\Lambda\ \bar{\Lambda}$ reconstruction	1.8
5C kinematic fit	1.1
$\Sigma^0\bar{\Sigma}^0$ mass window	0.1
Veto $\pi^+\pi^- J/\psi$	Negligible
Veto $\pi^0\pi^0 J/\psi$	4.1
Fit range	Negligible
Signal shape	1.6
Background shape	0.6
Signal MC sample size	0.7
Generator model	7.0
ω branching fraction	0.8
$\Lambda\ \bar{\Lambda}$ branching fraction	1.6
π^0 branching fraction	Negligible
Total number of $\psi(3686)$ events	0.5
Total	9.2

The uncertainty related to π^0 reconstruction is momentum-dependent, following the relation $(0.06 - 2.41 \times \frac{p}{\mathrm{GeV}/c})\%$ for a single π^0, where p is the π^0 momentum. This relation is obtained with the control samples $\psi(3686) \to \pi^0\pi^0 J/\psi$ and $e^+e^- \to \omega\pi^0$ at $\sqrt{s} = 3.773$ GeV [34]. In the signal decay, the momentum of the π^0 is distributed around 0.3 GeV$/c$. The momentum-weighted uncertainty, 1.0%, is assigned as the systematic uncertainty.

The differences in Λ and $\bar{\Lambda}$ reconstruction efficiency, including the tracking and PID of $p\pi$, as well as their decay length and mass windows, are studied using the control sample $J/\psi \to pK^-\bar{\Lambda} + \mathrm{c.c.}$ [35]. After correcting the signal efficiencies based on the data-MC difference, the residual uncertainties are assigned as the corresponding systematic uncertainties, each being 0.9% for both Λ and $\bar{\Lambda}$. Assuming the uncertainties of Λ and $\bar{\Lambda}$ reconstruction to be fully correlated, the overall systematic uncertainty due to Λ and $\bar{\Lambda}$ reconstruction is determined to be 1.8%.

The uncertainty associated with the 5C kinematic fit is estimated by comparing the efficiency with and without helix parameter corrections, following the method described in Ref. [36]. The difference in the signal efficiency, 1.1%, is assigned as the systematic uncertainty.

The uncertainty of the correlated 2-D $\Sigma^0\bar{\Sigma}^0$ mass window is estimated using the control sample of $J/\psi \to \Sigma^0\bar{\Sigma}^0$. The difference in the acceptance efficiency between the data and MC simulation, 0.1%, is account for the systematic uncertainty. The uncertainties associated with vetoing $\psi(3686) \to \pi^+\pi^-(\pi^0\pi^0)J/\psi$ events are estimated using the Barlow test [37]. We modify the nominal J/ψ mass windows by reducing or expanding them five times with increments of ± 2 MeV$/c^2$, then re-measure the branching fraction for each adjusted mass window. The test variable is defined as $\zeta = \frac{|V_{\mathrm{nominal}} - V_{\mathrm{test}}|}{\sqrt{|\sigma^2_{\mathrm{Vnominal}} - \sigma^2_{\mathrm{Vtest}}|}}$, where V_{nominal} denotes the nominal branching fraction result, V_{test} denotes the branching fraction from a specific mass window, $\sigma_{\mathrm{Vnominal}}$ and σ_{Vtest} are the statistical uncertainty of the nominal branching fraction and the uncertainty corresponding to V_{test}, respectively. If $\zeta < 2$ for all mass windows, the difference in the measured branching fractions is considered to be due to statistical fluctuations, rendering the uncertainty negligible. Otherwise, the largest difference in the measured branching fraction, corresponding to the highest value of ζ, is taken as the uncertainty.

The uncertainty of the fit range is found to be negligible using the Barlow test. The uncertainty arising from the signal shape is estimated by substituting the signal function derived from the simulated shape with a double Gaussian function. The difference in the fitted signal yield, amounting to 1.6%, is taken as the systematic uncertainty. The uncertainty related to the background function is estimated by replacing the Chebyshev polynomial function with the 2-D $\Sigma^0\bar{\Sigma}^0$ sideband. The difference in the fitted signal yield, 0.6%, is considered as the uncertainty.

The uncertainty associated with the MC model is estimated by using the data-driven `BODY3` [21] generator to regenerate a signal MC sample of equivalent size as the nominal signal MC sample. The Dalitz plot of $M^2_{\Sigma^0\omega}$ versus $M^2_{\bar{\Sigma}^0\omega}$ is input into the `BODY3` generator, with backgrounds subtracted using the ω sideband. The efficiency difference between the alternative and nominal MC samples, 7.0%, is assigned as a systematic uncertainty.

The uncertainty due to the limited signal MC sample size is calculated as $\sqrt{\frac{1-\varepsilon}{N\cdot\varepsilon}} = 0.7\%$, where ε is the efficiency and N is the total number of generated MC events.

The uncertainties for $\mathcal{B}(\Lambda \to p\pi^-/\bar{\Lambda} \to \bar{p}\pi^+)$ and $\mathcal{B}(\omega \to \pi^+\pi^-\pi^0)$ are sourced from the PDG [23], which are 0.8% for each decay. The uncertainty of $\mathcal{B}(\pi^0 \to \gamma\gamma)$ is considered negligible.

The uncertainty associated with the total number of $\psi(3686)$ events is 0.5% [9].

VII. SUMMARY

Using $(27.12 \pm 0.14) \times 10^8$ $\psi(3686)$ events collected by the BESIII detector in 2009, 2012 and 2021, we report the first observation of the decay $\psi(3686) \to \Sigma^0\bar{\Sigma}^0\omega$ with a statistical significance of 8.9σ. The branching fraction is measured to be $(1.24 \pm 0.16_{\mathrm{stat}} \pm 0.11_{\mathrm{sys}}) \times 10^{-5}$. This result is consistent with the previous measurement of its isospin partner process, $\psi(3686) \to \Sigma^+\bar{\Sigma}^-\omega$ [34], which was found to be $(1.89 \pm 0.18_{\mathrm{stat}} \pm 0.21_{\mathrm{sys}}) \times 10^{-5}$. Isospin symmetry predicts a branching fraction ratio of 1 between these two channels, and the measured result is consistent with this expectation at a 2σ uncertainty level. We also investigate potential structures in the invariant mass distributions of $\Sigma^0\omega$, $\bar{\Sigma}^0\omega$ and $\Sigma^0\bar{\Sigma}^0$. A hint of a resonance in the $M_{\Sigma^0(\bar{\Sigma}^0)\omega}$ spectrum is observed with a significance of 2.5σ. However, due to the limited statistics, we do not consider possible interference effects, and detailed information about the intermediate state, including its quantum numbers, cannot be determined.

ACKNOWLEDGMENTS

The BESIII Collaboration thanks the staff of BEPCII [38] and the IHEP computing center for their strong support. This work is supported in part by National Key R&D Program of China under Contracts No. 2020YFA0406300, No. 2020YFA0406400, No. 2023YFA1606000, and No. 2023YFA1606704; National Natural Science Foundation of China (NSFC) under Contracts No. 11635010, No. 11735014, No. 11935015, No. 11935016, No. 11935018, No. 12025502, No. 12035009, No. 12035013, No. 12061131003, No. 12192260, No. 12192261, No. 12192262, No. 12192263, No. 12192264, No. 12192265, No. 12221005, No. 12225509, No. 12235017, and No. 12361141819; the Chinese Academy of Sciences (CAS) Large-Scale Scientific Facility Program; the CAS Center for Excellence in Particle Physics (CCEPP); Joint Large-Scale Scientific Facility Funds of the NSFC and CAS under Contract No. U1832207; CAS under Contract No. YSBR-101; 100 Talents Program of CAS; The Institute of Nuclear and Particle Physics (INPAC) and Shanghai Key Laboratory for Particle Physics and Cosmology; Agencia Nacional de Investigación y Desarrollo de Chile (ANID), Chile under Contract No. ANID PIA/APOYO AFB230003; German Research Foundation DFG under Contract No. FOR5327; Istituto Nazionale di Fisica Nucleare, Italy; Knut and Alice Wallenberg Foundation under Contracts No. 2021.0174, No. 2021.0299; Ministry of Development of Turkey under Contract No. DPT2006K-120470; National Research Foundation of Korea under Contract No. NRF-2022R1A2C1092335; National Science and Technology fund of Mongolia; National Science Research and Innovation Fund (NSRF) via the Program Management Unit for Human Resources & Institutional Development, Research and Innovation of Thailand under Contract No. B50G670107; Polish National Science Centre under Contract No. 2019/35/O/ST2/02907; Swedish Research Council under Contract No. 2019.04595; The Swedish Foundation for International Cooperation in Research and Higher Education under Contract No. CH2018-7756; U.S. Department of Energy under Contract No. DE-FG02-05ER41374.

DATA AVAILABILITY

The data that support the findings of this article are not publicly available upon publication because it is not technically feasible and/or the cost of preparing, depositing, and hosting the data would be prohibitive within the terms of this research project. The data are available from the authors upon reasonable request.

[1] D. M. Asner *et al.*, Int. J. Mod. Phys. A **24**, S1 (2009).
[2] N. Brambilla *et al.*, Eur. Phys. J. C **71**, 1534 (2011).
[3] V. Crede, AIP Conf. Proc. **2249**, 020003 (2020).
[4] A. V. Sarantsev, M. Matveev, V. A. Nikonov, A. V. Anisovich, U. Thoma, and E. Klempt, Eur. Phys. J. A **55**, 180 (2019).
[5] C. Fernández-Ramírez, I. V. Danilkin, D. M. Manley, V. Mathieu, and A. P. Szczepaniak, Phys. Rev. D **93**, 034029 (2016).
[6] M. Ablikim *et al.* (BESIII Collaboration), Phys. Rev. D **106**, 072006 (2022).
[7] M. Ablikim *et al.* (BESIII Collaboration), Phys. Rev. D **106**, 112011 (2022).
[8] M. Ablikim *et al.* (BESIII Collaboration), Phys. Rev. D **104**, 052006 (2021).
[9] M. Ablikim *et al.* (BESIII Collaboration), Chin. Phys. C **48**, 093001 (2024).
[10] M. Ablikim *et al.* (BESIII Collaboration), Nucl. Instrum. Methods Phys. Res., Sect. A **614**, 345 (2010).
[11] C. H. Yu *et al.*, *Proceedings of IPAC2016*, Busan, Korea (JACoW, Geneva, Switzerland, 2016).
[12] M. Ablikim *et al.* (BESIII Collaboration), Chin. Phys. C **44**, 040001 (2020).
[13] J. W. Zhang *et al.*, Radiat. Detect. Technol. Methods **6**, 289 (2022).
[14] X. Li *et al.*, Radiat. Detect. Technol. Method **1**, 13 (2017).
[15] Y. X. Guo *et al.*, Radiat. Detect. Technol. Method **1**, 15 (2017).
[16] P. Cao *et al.*, Nucl. Instrum. Methods Phys. Res., Sect. A **953**, 163053 (2020).
[17] S. Agostinelli *et al.* (GEANT4 Collaboration), Nucl. Instrum. Methods Phys. Res., Sect. A **506**, 250 (2003).
[18] K. X. Huang *et al.*, Nucl. Sci. Tech. **33**, 142 (2022).
[19] S. Jadach, B. F. L. Ward, and Z. Was, Comput. Phys. Commun. **130**, 260 (2000).
[20] S. Jadach, B. F. L. Ward, and Z. Was, Phys. Rev. D **63**, 113009 (2001).
[21] R. G. Ping, Chin. Phys. C **32**, 599 (2008).

[22] D. J. Lange, Nucl. Instrum. Methods Phys. Res., Sect. A **462**, 152 (2001).
[23] S. Navas *et al.* (Particle Data Group), Phys. Rev. D **110**, 030001 (2024).
[24] J. C. Chen, G. S. Huang, X. R. Qi, D. H. Zhang, and Y. S. Zhu, Phys. Rev. D **62**, 034003 (2000).
[25] R. L. Yang, R. G. Ping, and H. Chen, Chin. Phys. Lett. **31**, 061301 (2014).
[26] E. Richter-Was, Phys. Lett. B **303**, 163 (1993).
[27] M. Ablikim *et al.* (BESIII Collaboration), Phys. Rev. Lett. **133**, 101902 (2024).
[28] X. Y. Zhou, S. X. Du, G. Li, and C. P. Shen, Comput. Phys. Commun. **258**, 107540 (2021).
[29] R. Barlow, Nucl. Instrum. Methods Phys. Res., Sect. A **297**, 496 (1990).
[30] K. S. Cranmer, Comput. Phys. Commun. **136**, 3 (2001).
[31] O. Vitells and E. Gross, Astropart. Phys. **35**, 230 (2011).
[32] M. Ablikim *et al.* (BESIII Collaboration), Phys. Rev. D **87**, 012007 (2013).
[33] M. Ablikim *et al.* (BESIII Collaboration), Phys. Rev. D **109**, 032006 (2024).
[34] M. Ablikim *et al.* (BESIII Collaboration), Phys. Rev. D **108**, 092011 (2023).
[35] M. Ablikim *et al.* (BESIII Collaboration), Phys. Rev. D **108**, 112012 (2023).
[36] M. Ablikim *et al.* (BESIII Collaboration), Phys. Rev. D **87**, 012002 (2013).
[37] O. Behnke, K. Kroninger, G. Schott, and T. Schörner-Sadenius, How to deal with systematic uncertainties, in *Data Analysis in High Energy Physics: A Practical Guide to Statistical Methods* (Wiley-VCH, Berlin, 2013).
[38] https://cstr.cn/31109.02.BEPC

Correction: A minor error in Eq. (2) has been fixed.

M. Ablikim,[1] M. N. Achasov,[4,c] P. Adlarson,[77] X. C. Ai,[82] R. Aliberti,[36] A. Amoroso,[76a,76c] Q. An,[73,59,a] Y. Bai,[58] O. Bakina,[37] Y. Ban,[47,h] H.-R. Bao,[65] V. Batozskaya,[1,45] K. Begzsuren,[33] N. Berger,[36] M. Berlowski,[45] M. Bertani,[29a] D. Bettoni,[30a] F. Bianchi,[76a,76c] E. Bianco,[76a,76c] A. Bortone,[76a,76c] I. Boyko,[37] R. A. Briere,[5] A. Brueggemann,[70] H. Cai,[78] M. H. Cai,[39,k,l] X. Cai,[1,59] A. Calcaterra,[29a] G. F. Cao,[1,65] N. Cao,[1,65] S. A. Cetin,[63a] X. Y. Chai,[47,h] J. F. Chang,[1,59] G. R. Che,[44] Y. Z. Che,[1,59,65] G. Chelkov,[37,b] C. H. Chen,[9] Chao Chen,[56] G. Chen,[1] H. S. Chen,[1,65] H. Y. Chen,[21] M. L. Chen,[1,59,65] S. J. Chen,[43] S. L. Chen,[46] S. M. Chen,[62] T. Chen,[1,65] X. R. Chen,[32,65] X. T. Chen,[1,65] Y. B. Chen,[1,59] Y. Q. Chen,[16] Y. Q. Chen,[35] Z. J. Chen,[26,i] Z. K. Chen,[60] S. K. Choi,[10] X. Chu,[12,g] G. Cibinetto,[30a] F. Cossio,[76c] J. Cottee-Meldrum,[64] J. J. Cui,[51] H. L. Dai,[1,59] J. P. Dai,[80] A. Dbeyssi,[19] R. E. de Boer,[3] D. Dedovich,[37] C. Q. Deng,[74] Z. Y. Deng,[1] A. Denig,[36] I. Denysenko,[37] M. Destefanis,[76a,76c] F. De Mori,[76a,76c] B. Ding,[68,1] X. X. Ding,[47,h] Y. Ding,[41] Y. Ding,[35] Y. X. Ding,[31] J. Dong,[1,59] L. Y. Dong,[1,65] M. Y. Dong,[1,59,65] X. Dong,[78] M. C. Du,[1] S. X. Du,[82] S. X. Du,[12,g] Y. Y. Duan,[56] Z. H. Duan,[43] P. Egorov,[37,b] G. F. Fan,[43] J. J. Fan,[20] Y. H. Fan,[46] J. Fang,[1,59] J. Fang,[60] S. S. Fang,[1,65] W. X. Fang,[1] Y. Q. Fang,[1,59] R. Farinelli,[30a] L. Fava,[76b,76c] F. Feldbauer,[3] G. Felici,[29a] C. Q. Feng,[73,59] J. H. Feng,[16] L. Feng,[39,k,l] Q. X. Feng,[39,k,l] Y. T. Feng,[73,59] M. Fritsch,[3] C. D. Fu,[1] J. L. Fu,[65] Y. W. Fu,[1,65] H. Gao,[65] X. B. Gao,[42] Y. N. Gao,[47,h] Y. N. Gao,[20] Y. Y. Gao,[31] Yang Gao,[73,59] S. Garbolino,[76c] I. Garzia,[30a,30b] P. T. Ge,[20] Z. W. Ge,[43] C. Geng,[60] E. M. Gersabeck,[69] A. Gilman,[71] K. Goetzen,[13] J. D. Gong,[35] L. Gong,[41] W. X. Gong,[1,59] W. Gradl,[36] S. Gramigna,[30a,30b] M. Greco,[76a,76c] M. H. Gu,[1,59] Y. T. Gu,[15] C. Y. Guan,[1,65] A. Q. Guo,[32] L. B. Guo,[42] M. J. Guo,[51] R. P. Guo,[50] Y. P. Guo,[12,g] A. Guskov,[37,b] J. Gutierrez,[28] K. L. Han,[65] T. T. Han,[1] F. Hanisch,[3] K. D. Hao,[73,59] X. Q. Hao,[20] F. A. Harris,[67] K. K. He,[56] K. L. He,[1,65] F. H. Heinsius,[3] C. H. Heinz,[36] Y. K. Heng,[1,59,65] C. Herold,[61] T. Holtmann,[3] P. C. Hong,[35] G. Y. Hou,[1,65] X. T. Hou,[1,65] Y. R. Hou,[65] Z. L. Hou,[1] H. M. Hu,[1,65] J. F. Hu,[57,j] Q. P. Hu,[73,59] S. L. Hu,[12,g] T. Hu,[1,59,65] Y. Hu,[1] Z. M. Hu,[60] G. S. Huang,[73,59] K. X. Huang,[60] L. Q. Huang,[32,65] P. Huang,[43] X. T. Huang,[51] Y. P. Huang,[1] Y. S. Huang,[60] T. Hussain,[75] N. Hüsken,[36] N. in der Wiesche,[70] J. Jackson,[28] S. Janchiv,[33] Q. Ji,[1] Q. P. Ji,[20] W. Ji,[1,65] X. B. Ji,[1,65] X. L. Ji,[1,59] Y. Y. Ji,[51] Z. K. Jia,[73,59] D. Jiang,[1,65] H. B. Jiang,[78] P. C. Jiang,[47,h] S. J. Jiang,[9] T. J. Jiang,[17] X. S. Jiang,[1,59,65] Y. Jiang,[65] J. B. Jiao,[51] J. K. Jiao,[35] Z. Jiao,[24] S. Jin,[43] Y. Jin,[68] M. Q. Jing,[1,65] X. M. Jing,[65] T. Johansson,[77] S. Kabana,[34] N. Kalantar-Nayestanaki,[66] X. L. Kang,[9] X. S. Kang,[41] M. Kavatsyuk,[66] B. C. Ke,[82] V. Khachatryan,[28] A. Khoukaz,[70] R. Kiuchi,[1] O. B. Kolcu,[63a] B. Kopf,[3] M. Kuessner,[3] X. Kui,[1,65] N. Kumar,[27] A. Kupsc,[45,77] W. Kühn,[38] Q. Lan,[74] W. N. Lan,[20] T. T. Lei,[73,59] M. Lellmann,[36] T. Lenz,[36] C. Li,[44] C. Li,[48] C. H. Li,[40] C. K. Li,[21] Cheng Li,[73,59] D. M. Li,[82] F. Li,[1,59] G. Li,[1] H. B. Li,[1,65] H. J. Li,[20] H. N. Li,[57,j] Hui Li,[44] J. R. Li,[62] J. S. Li,[60] K. Li,[1] K. L. Li,[39,k,l] K. L. Li,[20] L. J. Li,[1,65] Lei Li,[49] M. H. Li,[44] M. R. Li,[1,65] P. L. Li,[65] P. R. Li,[39,k,l] Q. M. Li,[1,65] Q. X. Li,[51] R. Li,[18,32] T. Li,[51] T. Y. Li,[44] W. D. Li,[1,65] W. G. Li,[1,a] X. Li,[1,65] X. H. Li,[73,59] X. L. Li,[51] X. Y. Li,[1,8] X. Z. Li,[60] Y. Li,[20] Y. G. Li,[47,h] Y. P. Li,[35] Z. J. Li,[60] Z. Y. Li,[80] C. Liang,[43] H. Liang,[73,59] Y. F. Liang,[55] Y. T. Liang,[32,65] G. R. Liao,[14] L. B. Liao,[60] M. H. Liao,[60] Y. P. Liao,[1,65] J. Libby,[27] A. Limphirat,[61] C. C. Lin,[56] C. X. Lin,[65] D. X. Lin,[32,65] L. Q. Lin,[40] T. Lin,[1] B. J. Liu,[1] B. X. Liu,[78] C. Liu,[35] C. X. Liu,[1] F. Liu,[1] F. H. Liu,[54] Feng Liu,[6] G. M. Liu,[57,j] H. Liu,[39,k,l] H. B. Liu,[15] H. H. Liu,[1] H. M. Liu,[1,65] Huihui Liu,[22] J. B. Liu,[73,59] J. J. Liu,[21] K. Liu,[74] K. Liu,[39,k,l]

K. Y. Liu,[41] Ke Liu,[23] L. Liu,[73,59] L. C. Liu,[44] Lu Liu,[44] P. L. Liu,[1] Q. Liu,[65] S. B. Liu,[73,59] T. Liu,[12,g] W. K. Liu,[44] W. M. Liu,[73,59] W. T. Liu,[40] X. Liu,[40] X. Liu,[39,k,l] X. K. Liu,[39,k,l] X. Y. Liu,[78] Y. Liu,[82] Y. Liu,[82] Y. Liu,[39,k,l] Y. B. Liu,[44] Z. A. Liu,[1,59,65] Z. D. Liu,[9] Z. Q. Liu,[51] X. C. Lou,[1,59,65] F. X. Lu,[60] H. J. Lu,[24] J. G. Lu,[1,59] X. L. Lu,[16] Y. Lu,[7] Y. H. Lu,[1,65] Y. P. Lu,[1,59] Z. H. Lu,[1,65] C. L. Luo,[42] J. R. Luo,[60] J. S. Luo,[1,65] M. X. Luo,[81] T. Luo,[12,g] X. L. Luo,[1,59] Z. Y. Lv,[23] X. R. Lyu,[65,p] Y. F. Lyu,[44] Y. H. Lyu,[82] F. C. Ma,[41] H. Ma,[80] H. L. Ma,[1] J. L. Ma,[1,65] L. L. Ma,[51] L. R. Ma,[68] Q. M. Ma,[1] R. Q. Ma,[1,65] R. Y. Ma,[20] T. Ma,[73,59] X. T. Ma,[1,65] X. Y. Ma,[1,59] Y. M. Ma,[32] F. E. Maas,[19] I. MacKay,[71] M. Maggiora,[76a,76c] S. Malde,[71] H. X. Mao,[39,k,l] Y. J. Mao,[47,h] Z. P. Mao,[1] S. Marcello,[76a,76c] A. Marshall,[64] F. M. Melendi,[30a,30b] Y. H. Meng,[65] Z. X. Meng,[68] J. G. Messchendorp,[13,66] G. Mezzadri,[30a] H. Miao,[1,65] T. J. Min,[43] R. E. Mitchell,[28] X. H. Mo,[1,59,65] B. Moses,[28] N. Yu. Muchnoi,[4,c] J. Muskalla,[36] Y. Nefedov,[37] F. Nerling,[19,e] L. S. Nie,[21] I. B. Nikolaev,[4,c] Z. Ning,[1,59] S. Nisar,[11,m] Q. L. Niu,[39,k,l] W. D. Niu,[12,g] C. Normand,[64] S. L. Olsen,[10,65] Q. Ouyang,[1,59,65] S. Pacetti,[29b,29c] X. Pan,[56] Y. Pan,[58] A. Pathak,[10] Y. P. Pei,[73,59] M. Pelizaeus,[3] H. P. Peng,[73,59] X. J. Peng,[39,k,l] Y. Y. Peng,[39,k,l] K. Peters,[13,e] K. Petridis,[64] J. L. Ping,[42] R. G. Ping,[1,65] S. Plura,[36] V. Prasad,[34] F. Z. Qi,[1] H. R. Qi,[62] M. Qi,[43] S. Qian,[1,59] W. B. Qian,[65] C. F. Qiao,[65] J. H. Qiao,[20] J. J. Qin,[74] J. L. Qin,[56] L. Q. Qin,[14] L. Y. Qin,[73,59] P. B. Qin,[74] X. P. Qin,[12,g] X. S. Qin,[51] Z. H. Qin,[1,59] J. F. Qiu,[1] Z. H. Qu,[74] J. Rademacker,[64] C. F. Redmer,[36] A. Rivetti,[76c] M. Rolo,[76c] G. Rong,[1,65] S. S. Rong,[1,65] F. Rosini,[29b,29c] Ch. Rosner,[19] M. Q. Ruan,[1,59] N. Salone,[45] A. Sarantsev,[37,d] Y. Schelhaas,[36] K. Schoenning,[77] M. Scodeggio,[30a] K. Y. Shan,[12,g] W. Shan,[25] X. Y. Shan,[73,59] Z. J. Shang,[39,k,l] J. F. Shangguan,[17] L. G. Shao,[1,65] M. Shao,[73,59] C. P. Shen,[12,g] H. F. Shen,[1,8] W. H. Shen,[65] X. Y. Shen,[1,65] B. A. Shi,[65] H. Shi,[73,59] J. L. Shi,[12,g] J. Y. Shi,[1] S. Y. Shi,[74] X. Shi,[1,59] H. L. Song,[73,59] J. J. Song,[20] T. Z. Song,[60] W. M. Song,[35] Y. X. Song,[47,h,n] S. Sosio,[76a,76c] S. Spataro,[76a,76c] F. Stieler,[36] S. S. Su,[41] Y. J. Su,[65] G. B. Sun,[78] G. X. Sun,[1] H. Sun,[65] H. K. Sun,[1] J. F. Sun,[20] K. Sun,[62] L. Sun,[78] S. S. Sun,[1,65] T. Sun,[52,f] Y. C. Sun,[78] Y. H. Sun,[31] Y. J. Sun,[73,59] Y. Z. Sun,[1] Z. Q. Sun,[1,65] Z. T. Sun,[51] C. J. Tang,[55] G. Y. Tang,[1] J. Tang,[60] L. F. Tang,[40] M. Tang,[73,59] Y. A. Tang,[78] L. Y. Tao,[74] M. Tat,[71] J. X. Teng,[73,59] J. Y. Tian,[73,59] W. H. Tian,[60] Y. Tian,[32] Z. F. Tian,[78] I. Uman,[63b] B. Wang,[1] B. Wang,[60] Bo Wang,[73,59] C. Wang,[39,k,l] C. Wang,[20] Cong Wang,[23] D. Y. Wang,[47,h] H. J. Wang,[39,k,l] J. J. Wang,[78] K. Wang,[1,59] L. L. Wang,[1] L. W. Wang,[35] M. Wang,[51] M. Wang,[73,59] N. Y. Wang,[65] S. Wang,[12,g] T. Wang,[12,g] T. J. Wang,[44] W. Wang,[74] W. Wang,[60] W. P. Wang,[36,59,73,o] X. Wang,[47,h] X. F. Wang,[39,k,l] X. J. Wang,[40] X. L. Wang,[12,g] X. N. Wang,[1] Y. Wang,[62] Y. D. Wang,[46] Y. F. Wang,[1,59,65] Y. H. Wang,[39,k,l] Y. L. Wang,[20] Y. N. Wang,[78] Y. Q. Wang,[1] Yaqian Wang,[18] Yi Wang,[62] Yuan Wang,[18,32] Z. Wang,[1,59] Z. L. Wang,[74] Z. L. Wang,[2] Z. Q. Wang,[12,g] Z. Y. Wang,[1,65] D. H. Wei,[14] H. R. Wei,[44] F. Weidner,[70] S. P. Wen,[1] Y. R. Wen,[40] U. Wiedner,[3] G. Wilkinson,[71] M. Wolke,[77] C. Wu,[40] J. F. Wu,[1,8] L. H. Wu,[1] L. J. Wu,[1,65] L. J. Wu,[20] Lianjie Wu,[20] S. G. Wu,[1,65] S. M. Wu,[65] X. Wu,[12,g] X. H. Wu,[35] Y. J. Wu,[32] Z. Wu,[1,59] L. Xia,[73,59] X. M. Xian,[40] B. H. Xiang,[1,65] D. Xiao,[39,k,l] G. Y. Xiao,[43] H. Xiao,[74] Y. L. Xiao,[12,g] Z. J. Xiao,[42] C. Xie,[43] K. J. Xie,[1,65] X. H. Xie,[47,h] Y. Xie,[51] Y. G. Xie,[1,59] Y. H. Xie,[6] Z. P. Xie,[73,59] T. Y. Xing,[1,65] C. F. Xu,[1,65] C. J. Xu,[60] G. F. Xu,[1] H. Y. Xu,[68,2] H. Y. Xu,[2] M. Xu,[73,59] Q. J. Xu,[17] Q. N. Xu,[31] T. D. Xu,[74] W. Xu,[1] W. L. Xu,[68] X. P. Xu,[56] Y. Xu,[12,g] Y. Xu,[41] Y. C. Xu,[79] Z. S. Xu,[65] H. Y. Yan,[40] L. Yan,[12,g] W. B. Yan,[73,59] W. C. Yan,[82] W. H. Yan,[6] W. P. Yan,[20] X. Q. Yan,[1,65] H. J. Yang,[52,f] H. L. Yang,[35] H. X. Yang,[1] J. H. Yang,[43] R. J. Yang,[20] T. Yang,[1] Y. Yang,[12,g] Y. F. Yang,[44] Y. H. Yang,[43] Y. Q. Yang,[9] Y. X. Yang,[1,65] Y. Z. Yang,[20] M. Ye,[1,59] M. H. Ye,[8] Z. J. Ye,[57,j] Junhao Yin,[44] Z. Y. You,[60] B. X. Yu,[1,59,65] C. X. Yu,[44] G. Yu,[13] J. S. Yu,[26,i] M. C. Yu,[41] T. Yu,[74] X. D. Yu,[47,h] Y. C. Yu,[82] C. Z. Yuan,[1,65] H. Yuan,[1,65] J. Yuan,[35] J. Yuan,[46] L. Yuan,[2] S. C. Yuan,[1,65] X. Q. Yuan,[1] Y. Yuan,[1,65] Z. Y. Yuan,[60] C. X. Yue,[40] Ying Yue,[20] A. A. Zafar,[75] S. H. Zeng,[64] X. Zeng,[12,g] Y. Zeng,[26,i] Y. J. Zeng,[60] Y. J. Zeng,[1,65] X. Y. Zhai,[35] Y. H. Zhan,[60] A. Q. Zhang,[1,65] B. L. Zhang,[1,65] B. X. Zhang,[1] D. H. Zhang,[44] G. Y. Zhang,[1,65] G. Y. Zhang,[20] H. Zhang,[82] H. Zhang,[73,59] H. C. Zhang,[1,59,65] H. H. Zhang,[60] H. Q. Zhang,[1,59,65] H. R. Zhang,[73,59] H. Y. Zhang,[1,59] J. Zhang,[82] J. Zhang,[60] J. J. Zhang,[53] J. L. Zhang,[21] J. Q. Zhang,[42] J. S. Zhang,[12,g] J. W. Zhang,[1,59,65] J. X. Zhang,[39,k,l] J. Y. Zhang,[1] J. Z. Zhang,[1,65] Jianyu Zhang,[65] L. M. Zhang,[62] Lei Zhang,[43] N. Zhang,[82] P. Zhang,[1,65] Q. Zhang,[20] Q. Y. Zhang,[35] R. Y. Zhang,[39,k,l] S. H. Zhang,[1,65] Shulei Zhang,[26,i] X. M. Zhang,[1] X. Y. Zhang,[41] X. Y. Zhang,[51] Y. Zhang,[74] Y. Zhang,[1] Y. T. Zhang,[82] Y. H. Zhang,[1,59] Y. M. Zhang,[40] Z. D. Zhang,[1] Z. H. Zhang,[1] Z. L. Zhang,[35] Z. L. Zhang,[56] Z. X. Zhang,[20] Z. Y. Zhang,[44] Z. Y. Zhang,[78] Z. Z. Zhang,[46] Zh. Zh. Zhang,[20] G. Zhao,[1] J. Y. Zhao,[1,65] J. Z. Zhao,[1,59] L. Zhao,[1] Lei Zhao,[73,59] M. G. Zhao,[44] N. Zhao,[80] R. P. Zhao,[65] S. J. Zhao,[82] Y. B. Zhao,[1,59] Y. L. Zhao,[56] Y. X. Zhao,[32,65] Z. G. Zhao,[73,59] A. Zhemchugov,[37,b] B. Zheng,[74] B. M. Zheng,[35] J. P. Zheng,[1,59] W. J. Zheng,[1,65] X. R. Zheng,[20] Y. H. Zheng,[65,p] B. Zhong,[42] C. Zhong,[20] H. Zhou,[36,51,o] J. Q. Zhou,[35] J. Y. Zhou,[35] S. Zhou,[6] X. Zhou,[78] X. K. Zhou,[6] X. R. Zhou,[73,59] X. Y. Zhou,[40] Y. Z. Zhou,[12,g] A. N. Zhu,[65]

J. Zhu,[44] K. Zhu,[1] K. J. Zhu,[1,59,65] K. S. Zhu,[12,g] L. Zhu,[35] L. X. Zhu,[65] S. H. Zhu,[72] T. J. Zhu,[12,g] W. D. Zhu,[42] W. D. Zhu,[12,g] W. J. Zhu,[1] W. Z. Zhu,[20] Y. C. Zhu,[73,59] Z. A. Zhu,[1,65] X. Y. Zhuang,[44] J. H. Zou,[1] and J. Zu[73,59]

(BESIII Collaboration)

[1]*Institute of High Energy Physics, Beijing 100049, People's Republic of China*
[2]*Beihang University, Beijing 100191, People's Republic of China*
[3]*Bochum Ruhr-University, D-44780 Bochum, Germany*
[4]*Budker Institute of Nuclear Physics SB RAS (BINP), Novosibirsk 630090, Russia*
[5]*Carnegie Mellon University, Pittsburgh, Pennsylvania 15213, USA*
[6]*Central China Normal University, Wuhan 430079, People's Republic of China*
[7]*Central South University, Changsha 410083, People's Republic of China*
[8]*China Center of Advanced Science and Technology, Beijing 100190, People's Republic of China*
[9]*China University of Geosciences, Wuhan 430074, People's Republic of China*
[10]*Chung-Ang University, Seoul 06974, Republic of Korea*
[11]*COMSATS University Islamabad, Lahore Campus, Defence Road, Off Raiwind Road, 54000 Lahore, Pakistan*
[12]*Fudan University, Shanghai 200433, People's Republic of China*
[13]*GSI Helmholtzcentre for Heavy Ion Research GmbH, D-64291 Darmstadt, Germany*
[14]*Guangxi Normal University, Guilin 541004, People's Republic of China*
[15]*Guangxi University, Nanning 530004, People's Republic of China*
[16]*Guangxi University of Science and Technology, Liuzhou 545006, People's Republic of China*
[17]*Hangzhou Normal University, Hangzhou 310036, People's Republic of China*
[18]*Hebei University, Baoding 071002, People's Republic of China*
[19]*Helmholtz Institute Mainz, Staudinger Weg 18, D-55099 Mainz, Germany*
[20]*Henan Normal University, Xinxiang 453007, People's Republic of China*
[21]*Henan University, Kaifeng 475004, People's Republic of China*
[22]*Henan University of Science and Technology, Luoyang 471003, People's Republic of China*
[23]*Henan University of Technology, Zhengzhou 450001, People's Republic of China*
[24]*Huangshan College, Huangshan 245000, People's Republic of China*
[25]*Hunan Normal University, Changsha 410081, People's Republic of China*
[26]*Hunan University, Changsha 410082, People's Republic of China*
[27]*Indian Institute of Technology Madras, Chennai 600036, India*
[28]*Indiana University, Bloomington, Indiana 47405, USA*
[29a]*INFN Laboratori Nazionali di Frascati, I-00044 Frascati, Italy*
[29b]*INFN Sezione di Perugia, I-06100 Perugia, Italy*
[29c]*University of Perugia I-06100, Perugia, Italy*
[30a]*INFN Sezione di Ferrara, I-44122 Ferrara, Italy*
[30b]*University of Ferrara, I-44122 Ferrara, Italy*
[31]*Inner Mongolia University, Hohhot 010021, People's Republic of China*
[32]*Institute of Modern Physics, Lanzhou 730000, People's Republic of China*
[33]*Institute of Physics and Technology, Mongolian Academy of Sciences, Peace Avenue 54B, Ulaanbaatar 13330, Mongolia*
[34]*Instituto de Alta Investigación, Universidad de Tarapacá, Casilla 7D, Arica 1000000, Chile*
[35]*Jilin University, Changchun 130012, People's Republic of China*
[36]*Johannes Gutenberg University of Mainz, Johann-Joachim-Becher-Weg 45, D-55099 Mainz, Germany*
[37]*Joint Institute for Nuclear Research, 141980 Dubna, Moscow region, Russia*
[38]*Justus-Liebig-Universitaet Giessen, II. Physikalisches Institut, Heinrich-Buff-Ring 16, D-35392 Giessen, Germany*
[39]*Lanzhou University, Lanzhou 730000, People's Republic of China*
[40]*Liaoning Normal University, Dalian 116029, People's Republic of China*
[41]*Liaoning University, Shenyang 110036, People's Republic of China*
[42]*Nanjing Normal University, Nanjing 210023, People's Republic of China*
[43]*Nanjing University, Nanjing 210093, People's Republic of China*
[44]*Nankai University, Tianjin 300071, People's Republic of China*
[45]*National Centre for Nuclear Research, Warsaw 02-093, Poland*
[46]*North China Electric Power University, Beijing 102206, People's Republic of China*
[47]*Peking University, Beijing 100871, People's Republic of China*
[48]*Qufu Normal University, Qufu 273165, People's Republic of China*

[49]*Renmin University of China, Beijing 100872, People's Republic of China*
[50]*Shandong Normal University, Jinan 250014, People's Republic of China*
[51]*Shandong University, Jinan 250100, People's Republic of China*
[52]*Shanghai Jiao Tong University, Shanghai 200240, People's Republic of China*
[53]*Shanxi Normal University, Linfen 041004, People's Republic of China*
[54]*Shanxi University, Taiyuan 030006, People's Republic of China*
[55]*Sichuan University, Chengdu 610064, People's Republic of China*
[56]*Soochow University, Suzhou 215006, People's Republic of China*
[57]*South China Normal University, Guangzhou 510006, People's Republic of China*
[58]*Southeast University, Nanjing 211100, People's Republic of China*
[59]*State Key Laboratory of Particle Detection and Electronics, Beijing 100049, Hefei 230026, People's Republic of China*
[60]*Sun Yat-Sen University, Guangzhou 510275, People's Republic of China*
[61]*Suranaree University of Technology, University Avenue 111, Nakhon Ratchasima 30000, Thailand*
[62]*Tsinghua University, Beijing 100084, People's Republic of China*
[63a]*Turkish Accelerator Center Particle Factory Group, Istinye University, 34010, Istanbul, Turkey*
[63b]*Near East University, Nicosia, North Cyprus, 99138, Mersin 10, Turkey*
[64]*University of Bristol, H H Wills Physics Laboratory, Tyndall Avenue, Bristol BS8 1TL, United Kingdom*
[65]*University of Chinese Academy of Sciences, Beijing 100049, People's Republic of China*
[66]*University of Groningen, NL-9747 AA Groningen, The Netherlands*
[67]*University of Hawaii, Honolulu, Hawaii 96822, USA*
[68]*University of Jinan, Jinan 250022, People's Republic of China*
[69]*University of Manchester, Oxford Road, Manchester M13 9PL, United Kingdom*
[70]*University of Muenster, Wilhelm-Klemm-Strasse 9, 48149 Muenster, Germany*
[71]*University of Oxford, Keble Road, Oxford OX13RH, United Kingdom*
[72]*University of Science and Technology Liaoning, Anshan 114051, People's Republic of China*
[73]*University of Science and Technology of China, Hefei 230026, People's Republic of China*
[74]*University of South China, Hengyang 421001, People's Republic of China*
[75]*University of the Punjab, Lahore-54590, Pakistan*
[76a]*University of Turin and INFN, University of Turin, I-10125 Turin, Italy*
[76b]*University of Eastern Piedmont, I-15121 Alessandria, Italy*
[76c]*INFN, I-10125 Turin, Italy*
[77]*Uppsala University, Box 516, SE-75120 Uppsala, Sweden*
[78]*Wuhan University, Wuhan 430072, People's Republic of China*
[79]*Yantai University, Yantai 264005, People's Republic of China*
[80]*Yunnan University, Kunming 650500, People's Republic of China*
[81]*Zhejiang University, Hangzhou 310027, People's Republic of China*
[82]*Zhengzhou University, Zhengzhou 450001, People's Republic of China*

[a]Deceased.
[b]Also at the Moscow Institute of Physics and Technology, Moscow 141700, Russia.
[c]Also at the Novosibirsk State University, Novosibirsk 630090, Russia.
[d]Also at the NRC "Kurchatov Institute," PNPI, 188300 Gatchina, Russia.
[e]Also at Goethe University Frankfurt, 60323 Frankfurt am Main, Germany.
[f]Also at Key Laboratory for Particle Physics, Astrophysics and Cosmology, Ministry of Education, Shanghai Key Laboratory for Particle Physics and Cosmology, Institute of Nuclear and Particle Physics, Shanghai 200240, People's Republic of China.
[g]Also at Key Laboratory of Nuclear Physics and Ion-beam Application (MOE) and Institute of Modern Physics, Fudan University, Shanghai 200443, People's Republic of China.
[h]Also at State Key Laboratory of Nuclear Physics and Technology, Peking University, Beijing 100871, People's Republic of China.
[i]Also at School of Physics and Electronics, Hunan University, Changsha 410082, China.
[j]Also at Guangdong Provincial Key Laboratory of Nuclear Science, Institute of Quantum Matter, South China Normal University, Guangzhou 510006, China.
[k]Also at MOE Frontiers Science Center for Rare Isotopes, Lanzhou University, Lanzhou 730000, People's Republic of China.
[l]Also at Lanzhou Center for Theoretical Physics, Lanzhou University, Lanzhou 730000, People's Republic of China.
[m]Also at the Department of Mathematical Sciences, IBA, Karachi 75270, Pakistan.
[n]Also at Ecole Polytechnique Federale de Lausanne (EPFL), CH-1015 Lausanne, Switzerland.
[o]Also at Helmholtz Institute Mainz, Staudinger Weg 18, D-55099 Mainz, Germany.
[p]Also at Hangzhou Institute for Advanced Study, University of Chinese Academy of Sciences, Hangzhou 310024, China.